

# Theory of Reciprocating Contact for Viscoelastic Solids

Carmine Putignano †, Giuseppe Carbone †‡§, and Daniele Dini †

†*Department of Mechanical Engineering,  
Imperial College London, London, United Kingdom*

‡*Department of Mechanics, Mathematics and Management, Politecnico di Bari, Bari, Italy and*  
§*CNR Institute for Photonics and Nanotechnologies U.O.S. Bari, Physics Department M. Merlin, Bari, Italy.*

A theory of reciprocating contacts for linear viscoelastic materials is presented. Results are discussed for the case of a rigid sphere sinusoidally driven in sliding contact with a viscoelastic half-space. Depending on the size of the contact, the frequency and amplitude of the reciprocating motion, and on the relaxation time of the viscoelastic body, we establish that the contact behavior may range from the steady-state viscoelastic solution, in which traction forces always oppose the direction of the sliding rigid punch, to a more elaborate trend, never observed before, which is due to the strong interaction between different regions of the path covered during the reciprocating motion. Practical implications span a number of applications, ranging from seismic engineering to biotechnology.

**PACS numbers:** 62.20.Qp , 46.55.+d , 46.35.+z.

## INTRODUCTION

The mechanics and physics of soft materials are intrinsically complex due to the strongly time-dependent and usually non-linear constitutive stress-strain relations that govern their response. Further intricacy is added when soft bodies are brought into contact and the problem is exacerbated by the geometry of the intimately mating surfaces. In the last two decades, the continuously growing technological relevance of engineering applications involving polymeric materials and soft tissues has generated enormous interest in the scientific community and has contributed to a leap in the number of publications in the field [1-3] ; these span investigations performed across the scales, from macroscopic to atomistic levels, and include analytical [4, 5] numerical [6, 7] and experimental [8, 9] studies. Surprisingly, in spite of these vast research efforts, our understanding of soft matter problems is definitely far from being complete.

In this paper, we focus our attention on an issue that has been systematically ignored but has a crucial importance: the reciprocating contact of viscoelastic materials, where the relative motion between the contacting bodies is periodically inverted. Indeed, researchers have almost universally developed models to investigate unidirectional steady-state sliding between two mating surfaces made of viscoelastic material [5, 7]. However, steady-state assumption cannot be considered a universally valid condition. There is a countless variety of engineering applications, ranging from the macro- to the nano- scales, where a periodic inversion of the motion direction is present. Earthquake viscoelastic dampers are a classic example [11]. These devices are embedded in civil structures to limit the consequences of earthquakes by introducing a source of damping, that is, beyond the several possible configurations, the hysteretic dissipation occurring when a set of rigid punches deforms a layer

of rubber. Currently, the design in this field mostly relies on practical and empirical guidelines, and no tool for quantitative predictions is available. This lack of a robust theoretical framework involves also very different components, like all the sealing systems in mechanical applications with an alternate motion [10]. Indeed, enhancing performances and efficiency is infeasible without an accurate knowledge of the interfacial stresses and, consequently, of the dissipated power. Finally, reciprocating contacts have prominence also at different scales and in different contexts, like biology and biotechnology ([13],[14]). Skin, ocular system, joints, spine and vertebrae are some of the examples where viscoelastic soft contact occurs in the human body. As recently suggested in Ref. [13], this can be observed up to the cell scale, thus introducing the concept of cell friction. Indeed, Ref. [13] shows experimental results for reciprocating contact tests on layers of epithelial cells: what is obtained in terms of friction cannot be explained with a simple elastic model and needs a specific theory.

The schematic in Fig. 1 captures the variety of surfaces whose function and/or performance can be ameliorated by shedding light on the principles governing the problem under investigation.

In this work, we develop a theoretical approach and a numerical technique that, for the first time, allow studying reciprocating contact mechanics between linearly viscoelastic solids and provide predictions of the response of the contacting surfaces in terms of stresses, strain and friction. The paper is outlined as follows. Section II describes the mathematical formulation which the numerical methodology relies on. Section III focuses on a simple, tough explicative, case, i.e. the reciprocating sliding contact of a sphere over a viscoelastic layer. Final remarks are included to comment on the relevance of the theory and of the results. Appendixes A and B respectively discuss the validity range of the model and provide

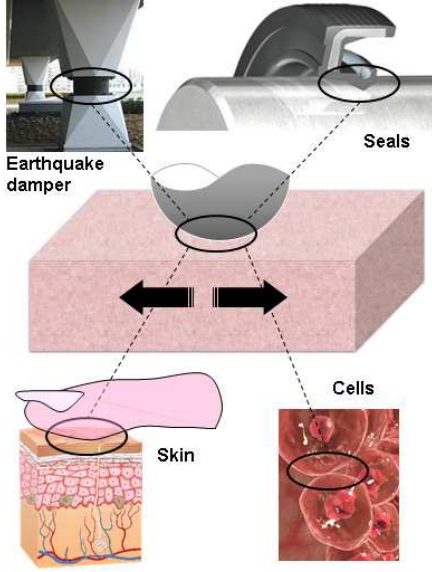


FIG. 1. Reciprocating viscoelastic contacts: schematic illustration showing relevant applications.

a comparison with steady-state conditions.

## FORMULATION

The proposed formulation builds on the strengths of the boundary element method (BEM) in terms of accurately capturing interfacial stresses and displacements, and, as such, requires the determination of a viscoelastic reciprocating Green's function  $G(\mathbf{x}, t)$ .

To this end, let us first assume that the interfacial normal stress distribution obeys the law  $\sigma(\mathbf{x}, t) = \sigma[\mathbf{x} - \xi_0 \sin(\omega t)]$ , i.e. that the shape of normal stress distribution is fixed but moves on the viscoelastic half-space with a sinusoidal law of amplitude  $|\xi_0|$  and angular frequency  $\omega$ . The vector  $\xi_0$  also identifies the direction of the reciprocating motion. Because of linearity and translational invariance, replacing  $\mathbf{x} \rightarrow \mathbf{x} + \xi_0 \sin(\omega t)$  allows to write the relation between interfacial stresses and displacement as

$$u(\mathbf{x}, t) = \int d^2x' G(\mathbf{x} - \mathbf{x}', t) \sigma(\mathbf{x}'). \quad (1)$$

In order to determine  $G(\mathbf{x}, t)$ , we recall that the general relation between stress and displacement fields is [7]:

$$u(\mathbf{x}, t) = \mathcal{J}(0) \int d^2x' \mathcal{G}(\mathbf{x} - \mathbf{x}') \sigma(\mathbf{x}', t) + \int_{-\infty}^t d\tau \dot{\mathcal{J}}(t - \tau) \int d^2x' \mathcal{G}(\mathbf{x} - \mathbf{x}') \sigma(\mathbf{x}', \tau), \quad (2)$$

where  $\mathcal{G}(\mathbf{x})$  and  $\mathcal{J}(t)$  are the elastic Green's function and the creep material function respectively. The symbol ' $\dot{\cdot}$ ' stands for the time derivative. The creep function is easily linked to the viscoelastic modulus  $E(\omega)$  of the material by means of the relation  $1/E(\omega) = i\omega\mathcal{J}(\omega)$  [15], where  $i$  is the imaginary unit and the Fourier transform of a function  $f(t)$  is  $f(\omega) = \int dt \exp(-i\omega t) f(t)$ . The viscoelastic modulus has the general expression  $1/E(\omega) = 1/E_\infty + \int_0^\infty d\tau \mathcal{C}(\tau) / (1 + i\omega\tau)$ , where  $E_\infty$  is a real quantity corresponding to the elastic modulus of the material at very large excitation frequencies.  $\mathcal{C}(\tau) > 0$  is usually defined as the creep spectrum, and  $\tau$  is the relaxation time [15]. In order to find  $G(\mathbf{x}, t)$  we choose  $\sigma(\mathbf{x}, t) = \delta[\mathbf{x} - \xi_0 \sin(\omega t)]$  and, after substituting in Eq. (2), we obtain

$$G(\mathbf{x}, t) = \mathcal{J}(0) \mathcal{G}[\mathbf{x} - \xi_0 \sin(\omega t)] + \int_{-\infty}^t d\tau \dot{\mathcal{J}}(t - \tau) \mathcal{G}[\mathbf{x} - \xi_0 \sin(\omega t)]. \quad (3)$$

The term  $\mathcal{G}[\mathbf{x} - \xi_0 \sin(\omega t)]$  can be re-written as

$$\mathcal{G}[\mathbf{x} - \xi_0 \sin(\omega t)] = (2\pi)^{-2} \int d^2q \mathcal{G}(\mathbf{q}) e^{-i\mathbf{q} \cdot [\mathbf{x} - \xi_0 \sin(\omega t)]}, \quad (4)$$

where  $\mathcal{G}(\mathbf{q})$  is the Fourier transform of the function  $\mathcal{G}(\mathbf{x})$ . Now, let us observe that  $\int d\theta e^{ir \sin \theta} e^{-i\alpha\theta}$  is equal to

$$\int d\theta e^{ir \sin \theta} e^{-i\alpha\theta} = 2\pi \sum_{k=-\infty}^{+\infty} \delta(\alpha - k) J_k(r), \quad (5)$$

where  $J_k(r)$  is the  $k$ -th order Bessel function of the first kind. Consequently, Eq. (4) can be casted as

$$\mathcal{G}[\mathbf{x} - \xi_0 \sin(\omega t)] = \sum_{k=-\infty}^{+\infty} A_k(\mathbf{x}) e^{ik\omega t}. \quad (6)$$

In Eq. (6),  $A_k(\mathbf{x})$  can be written as

$$A_k(\mathbf{x}) = (2\pi)^{-1} \int_{-1}^1 ds \mathcal{G}(\mathbf{x} - s\xi_0) B_k(s) \quad (7)$$

with  $B_k(s)$  being equal to  $B_k(s) = (-i)^k T_k(s) B_0(s)$ .  $T_k(s)$  is the Chebyshev polynomial of the first kind and  $B_0(s) = 2(1 - s^2)^{-1/2}$ , for  $|s| \leq 1$  and 0 otherwise. Substituting (6) in (3) we obtain:

$$G(\mathbf{x}, t) = \sum_{k=-\infty}^{+\infty} \frac{A_k(\mathbf{x})}{E(k\omega)} e^{ik\omega t}. \quad (8)$$

As mentioned above, the function  $G(\mathbf{x}, t)$  has been obtained under the assumption that the shape of the stress

field at the interface, whose general form is  $\sigma(\mathbf{x}, t) = \sigma[\mathbf{x} - \xi_0 \sin(\omega t), t]$ , does not change during the reciprocating motion, *i.e.*  $\sigma(\mathbf{x}, t) = \sigma[\mathbf{x} - \xi_0 \sin(\omega t)]$ . Such a condition holds true whenever  $a_0/|\xi_0| \ll 1$ , where  $a_0$  the characteristic dimension of the contact region, and is equivalent to require that  $|\partial\sigma/\partial t|/(|\xi_0 \cdot \nabla\sigma|\omega) \ll 1$  (see Appendix A for more details). This assumption is justified in the majority of cases of reciprocating contact,

$$u_i = \frac{1}{N} \sum_{j=1}^M \sigma_j \sum_{r=1}^N L \left[ \mathbf{x}_i - \mathbf{x}_j - \cos \left( \frac{2r-1}{2N} \pi \right) \xi_0 \right] \sum_{k=-\infty}^{+\infty} \frac{e^{ik\omega t} (-i)^k}{E(k\omega)} \cos \left[ k \left( \frac{2r-1}{2N} \pi \right) \right] \quad (9)$$

where  $L(\mathbf{x})$  is related to the Love's solution [16]. It should be observed that Eq. (9) is obtained by applying the Chebishev-Gauss quadrature rule to the integral term  $\int_{-1}^1 ds T_k(s) L[\mathbf{x}_i - \mathbf{x}'_j - s\xi_0] (1-s^2)^{-1/2}$  at  $M$  nodes, thus making it easier to achieve the numerical convergence of the problem.

Eq. (2) can be solved by using the iterative technique developed in Ref. [17] for elastic contacts, thus providing contact areas, stresses and strains. It should be noticed that the method does not require any discretization of the time domain as the time  $t$  is treated as a parameter.

Once the solution is known in terms of stresses and strains, following the approach stated in Ref. [7], it is straightforward to calculate the viscoelastic friction force as:

$$F_T = \int_D d^2x \sigma(\mathbf{x}) \frac{\partial u}{\partial x} \quad (10)$$

The friction coefficient is then obtained as  $\mu = F_T/F_N$  where  $F_N$  is the external applied load.

Finally, we conclude noticing that the formulation, in the current form, does not explicitly account for the role of the tangential tractions at the contact interface. Indeed, this is out of the scope of our work. The purpose of the paper is to determine the normal stresses and the normal displacements distribution, and, on this basis, calculate the viscoelastic friction that is proportional to the volume of deformed material. It is well known that the normal and tangential contact problems have only a very weak coupling, which is normally neglected [18]. Furthermore, in the case of a rigid body in contact with a soft layer—which can be usually assumed incompressible—, it is absolutely rigorous to assert that tractions has no influence on normal pressure and displacements, and, consequently, on the viscoelastic dissipation [18].

and is satisfied point-wise almost everywhere within the contact area in the analyses presented in this work. Now, to invert the linear operator in Eq. (1) we need a numerical approach which consists in discretizing the contact domain in  $M$  square cells. Indeed, assuming that in each boundary element the normal stress  $\sigma$  is constant and equal to  $\sigma_j$ , the normal displacement  $u_i = u(\mathbf{x}_i, t)$  at the centre  $\mathbf{x}_i$  of the  $i$ -th square can be written as:

## RESULTS AND DISCUSSION

We study the contact of a rigid sphere of radius  $R$  undergoing reciprocating sliding against a viscoelastic material characterized by one relaxation time ( being the ratio between the high frequency modulus and the low frequency  $E_\infty/E_0 = 11$  and the Poisson ratio  $\nu = 0.5$ ). We assume that the center  $\mathbf{x}(t)$  of the sphere moves on the viscoelastic half-space following the law  $\mathbf{x}(t) = [\xi_0 \sin(\omega t), 0]$ . The dimensionless angular frequency of the reciprocating motion is  $\omega\tau = 5$ , being  $\tau$  the relaxation time of the viscoelastic material.

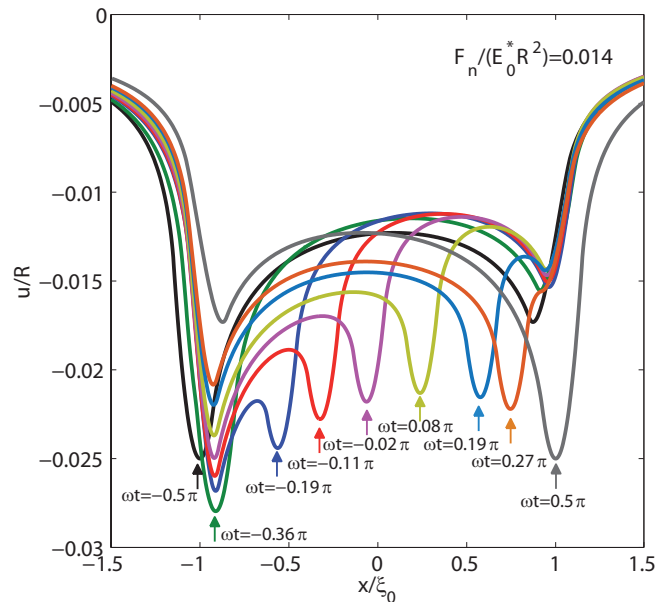


FIG. 2. The dimensionless normal displacements  $u(x, y = 0)/R$  as a function of the dimensionless abscissa  $x/\xi_0$  for a constant dimensionless normal force  $F_n/R^2 E_0^* = 0.014$ , for an amplitude  $\xi_0/R = 1$  and for several values of the dimensionless time  $\omega t \in [-\pi/2, \pi/2]$ .

Figure 2 shows the evolution of the dimensionless dis-

placements,  $u(x)/R$ , at the centre of the contact as a function of  $x/\xi_0$  and for a specific dimensionless applied normal load  $F_n/R^2E_0^* = 0.014$ , and  $\xi_0/R = 1$ . Results are shown for different values of  $\omega t \in [-\pi/2, \pi/2]$ . An arrow refers, in each case, to the current position of the sphere. At  $\omega t = -\pi/2$  the sphere has just reached the left dead-point and starts moving from left to right. Upon reversal of the sliding direction, and for  $\omega t \leq -0.36\pi$ , a marked increase of the dimensionless penetration at the center of the sphere is observed. This is due to the fact that, although the speed is increasing, it is still too low to cause a significant stiffening of the material, and the sphere is also moving over a portion of the viscoelastic half-space that has not yet had the time to relax after the previous contact of the rigid body. As the sliding speed increases, a non negligible stiffening of the material and a marked decrease of the penetration are observed (see displacement in correspondence to the arrow). This is clearly shown by curves at  $\omega t = -0.19\pi, -0.11\pi, -0.02\pi$ , which also show additional deformation peaks, one at the left and one to the right of the arrow: this is the result of the interplay between the deformations, induced by the indenter as it moves to the right, and the original not yet fully relaxed footprints left by the sphere at preceding times. For  $0 < \omega t < \pi/2$ , the sliding speed begins to decrease and the material softens again, thus leading to an increase of penetration. It is now possible to justify the occurrence of three different deformations peaks within the track when the sphere is moving between the two dead-ends: one corresponds to the current position of the sphere and the other two are located close to the left and right dead-points respectively, and are the result of the material inability to fully recover the viscoelastic deformations during a period of time comparable to the period  $T = 2\pi/\omega = 6.28$  s of the reciprocating motion (recall that the relaxation time is  $\tau = 5$  s).

The merging or separation of the previous and current sphere footprints, which takes place close to the dead-points of the reciprocating motion, has a significant effect on the interfacial normal stress distribution. This is clearly shown in Figure 3, which depicts the evolution of the pressure distribution and shows the shape of the contact area. Let us first observe that at  $\omega t = -\pi/2$ , *i.e.* when the sliding speed goes to zero, the contact area as well as the interfacial normal stress distribution are characterized by an asymmetric shape. The observed asymmetry and, in particular, the presence of a peak on the left of the contact patch is a consequence of the viscoelastic time-delay which prevents the material to relax immediately when the sliding speed vanishes. As the sphere starts moving to the right, such a peak cannot disappear suddenly but has to show a gradual decrease. At the same time, since the punch is travelling towards the right, as already observed in steady-state viscoelastic contacts moving at constant velocity [7], a peak in the pressure distribution has to be originated also at the leading edge

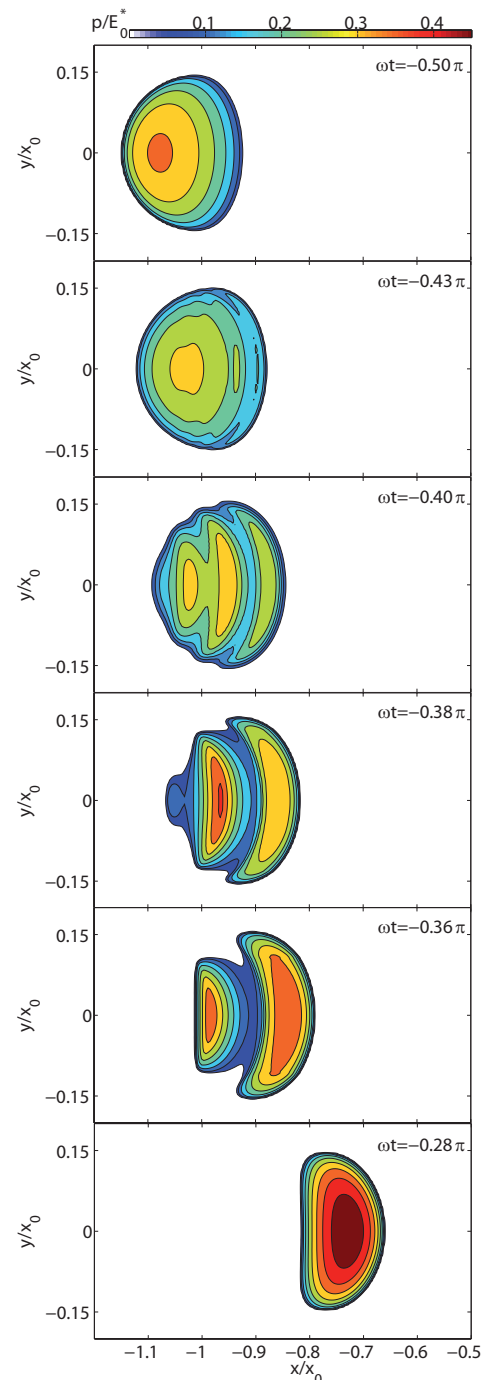


FIG. 3. The shape of the contact area and the contour plots of the normalised contact pressure distributions,  $p/E_0^*$ , for several values of  $\omega t$ .

. Finally, at the center of the distribution, where we have the maximum of the displacement field in the contact area, the pressure must still resemble the classical elastic Hertzian solution. All this process strongly affects the evolution of the pressure distribution at the interface with the presence of multiple pressure peaks shown

by the snapshots taken at  $\omega t = -0.40\pi, -0.38\pi, -0.36\pi$  (the reader may refer to Appendix B to appreciate the difference with steady-state conditions). A single peaked pressure distribution is later recovered: indeed, an asymmetric pressure profile marked by a peak closer to the contact leading edge is visible at  $\omega t = -0.28\pi$ .

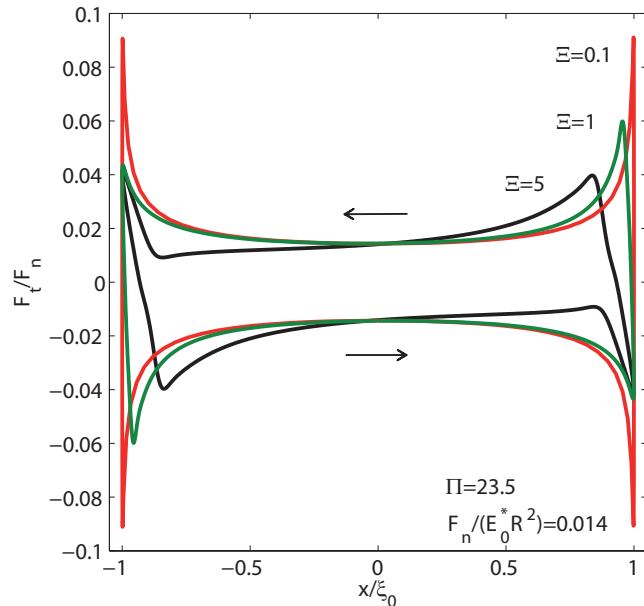


FIG. 4. The ratio between the tangential and the normal force  $F_t/F_n$  as a function of the dimensionless abscissa  $x/\xi_0$  for different values of  $\Xi$ . Arrows refer to the hysteresis cycle direction.

We may observe that, for a single relaxation time material, in addition to the ratio  $E_\infty/E_0$ , the behavior of the reciprocating contact is also governed by other two dimensionless parameters. The first dimensionless group is  $\Pi = \tau/t_0$ , where  $t_0 = a_0/\omega\xi_0$  and  $a_0$  is the Hertzian contact radius. This parameter can be also interpreted as a dimensionless sliding speed [7] and compares the relaxation time  $\tau$  with the time  $t_0$  needed by the sphere to cover a distance  $a_0$ . The second group,  $\Gamma = a_0/\xi_0 = \omega t_0 = 2\pi t_0/T$ , compares, instead, the time  $t_0$  with the period  $T = 2\pi/\omega$  of the reciprocating motion. Since we have earlier assumed that in our problem  $\Gamma = a_0/\xi_0 \ll 1$ , we can focus on observing how the solution is affected by  $\Pi$ . For extremely small or extremely high values of  $\Pi$ , the response of the system is elastic (governed by either the high or the low frequency elastic limit of the material), and no tangential contact force will be generated. At intermediate values of  $\Pi$ , viscoelasticity will affect the solution leading to asymmetric contact areas and pressure distributions, and to the generation of tangential contact forces. In such a case, given the dimensionless parameter  $\Xi = \Gamma \Pi = \omega\tau = 2\pi\tau/T$ , if  $\Xi < 1$ , the reciprocating motion will occur on time-scales longer than the relaxation time  $\tau$  of the material and the sys-

tem will resemble the steady-state behavior of the contact between a sphere moving on a viscoelastic half-space at constant speed [7]. If  $\Xi \approx 1$ , as in the case of Fig. 3, a strong interaction will be observed between different viscoelastic regions of the path covered by the sphere during the reciprocating motion. Note that, under the assumption small  $a_0/\xi_0$  values (which has been always adopted in this paper), the condition  $\Xi \gg 1$  implies  $\Pi \gg 1$ , and, in this case, the elastic response of the material will be recovered: the sphere will be just performing very fast oscillations, leading to a local stiffening and, ultimately, to a high frequency elastic behavior.

In Figure 4, the reduced tangential force,  $F_t/F_n$ , easily calculated once pressures and displacements are known [7], is plotted as a function of the dimensionless abscissa  $x/\xi_0$ , which identifies the position of the sphere along the path, for different values of  $\Xi$ . For  $\Xi = 0.1$  the material has the possibility to relax before a single reciprocating cycle is completed. In this case, as the solution resembles the steady-state viscoelastic sliding contact, the tangential force  $F_t/F_n$  always opposes the sphere speed at each point along the path. However, as  $\Xi$  is increased (see *e.g.* results for  $\Xi = 5$  presented in Figure 4) the relaxation of the material involves time scales comparable to the time period of the reciprocating motion; in this case, there exist regions on the sphere track, specifically those close to the dead-points, where  $F_t/F_n$  has the same direction as the sliding speed. This is perfectly consistent with the results presented in Figure 3.

## CONCLUSION

This work provides the explicit solution, in terms of a Fourier series, of the Green's function of the reciprocating contact problem between a rigid punch and a linear viscoelastic solid. The periodic features, intrinsically marking the problem, enables the parametric calculation of the contact solution for each time step without any necessity of employing the solution in the previous time interval. By implementing such a parametrically time-dependent approach, we obtain the full numerical convergence in each moment of the cycle and, interestingly, also when the punch inverts its motion.

For the simple case of a sphere in contact with a viscoelastic layer, we show that the behavior of the system is completely determined by two parameters, that are  $\Pi = \tau/t_0$  and  $\Xi = \omega\tau$ . Depending on these two parameters, the viscoelastic reciprocating contact may present a wide variety of different behaviors, ranging from the case that can be captured by the steady-state solution for viscoelastic sliding to the case where such interactions lead to the formation of a multi-peaked interfacial pressure distribution and tangential contact forces in (rather than opposing) the direction of the sliding speed.

This may have important implications in terms of de-

sign of materials and solutions for different applications as it would enable to accurately capture deformation rates, stress distributions and viscoelastic friction during reciprocation. Indeed, these are the key quantities to understand cell growth and skin/counterface interactions, as well as to predict frictional energy dissipation in *e.g.* mechanical seals and earthquake dampers.

### Appendix A: Comments on the parametrically time-dependent Boundary Element formulation

When dealing with materials marked by a linear response, the displacement distribution can be related to the interfacial pressures by means of a convolution integral with a time- and space-dependent function, i.e. the Green's function. We may, then, formulate the general contact problem between a rigid indenter and a linearly viscoelastic slab as:

$$u(\mathbf{x}, t) = \int_{-\infty}^t d\tau \int d^2x \mathcal{J}(t - \tau) \mathcal{G}(\mathbf{x} - \mathbf{x}') \dot{\sigma}(\mathbf{x}', \tau), \quad (11)$$

where  $\mathbf{x}$  is the in-plane position vector,  $t$  is the time,  $u(\mathbf{x}, t)$  is the normal surface displacement of the viscoelastic slab,  $\sigma(\mathbf{x}, t)$  is the normal interfacial stress,  $\mathcal{G}(\mathbf{x})$  and  $\mathcal{J}(t)$  are respectively the elastic Green's function and the creep material function. The relevance of such an approach is related to its generality: no assumption is made *a priori* on the shape of the contact domain. Indeed, the method can be employed for any kind of contact punch and even for rough surfaces: conditions, like periodic boundaries and finite values of contacting layers thickness, can be easily managed [19, 20]. Furthermore, since the creep function  $\mathcal{J}(t)$  is absolutely general, the approach is capable of dealing with any linearly viscoelastic material, from skin tissues to rubber-based composites.

However, solving directly Eq. (11) may be extremely challenging: due to the necessity of performing discretization both in time and space, the computational cost is huge and often infeasible with the computational technologies currently available. Consequently, when focusing our attention on the reciprocating contacts, our efforts are aimed at reducing the computational complexity of Eq. (11) without losing its generality in terms of contact geometry and material properties. Indeed, by assuming that the shape of the interfacial normal stress distribution does not change, i.e. assuming that it obeys the law  $\sigma(\mathbf{x}, t) = \sigma[\mathbf{x} - \xi_0 \sin(\omega t)]$  - where  $|\xi_0|$  and  $\omega$  are respectively the amplitude and angular frequency of the sinusoidal law-, Eq. (11) can be re-written in the form stated in Eq. (1). This expression has a significant advantage: it does not require any discretization of the time domain since  $t$  is present just as a parameter of the

viscoelastic reciprocating Green's function  $G(\mathbf{x}, t)$ . Such a formulation enables us to employ the efficient computational techniques already developed for the purely elastic case [17] and, therefore, to find the solution for a reciprocating contact. Incidentally, we observe that, from a physical point of view, passing from Eq. (11) to Eq. (1) is fully justified recalling the periodic features of the system under investigation.

In this paper, we determine  $G(\mathbf{x}, t)$  and investigate the main peculiarities of the reciprocating contact mechanics. Indeed, when developing the mathematical formulation, we rely on the aforementioned condition of a constant shape of the interfacial stress distribution. Recalling that the total time derivative of pressure field is  $\dot{\sigma} = \partial\sigma/\partial t + \mathbf{v} \cdot \nabla\sigma$ , the condition implies that, the local rate of change in the pressure  $\partial\sigma/\partial t$ , which occurs on time-scales of the order of the period  $T$  of the reciprocating motion, should be negligible compared to the rate of change of pressure due to the convective term  $\mathbf{v} \cdot \nabla\sigma$ , which occurs on time-scale of  $t_0$ , where  $t_0$  is the time needed by the sphere to cover a distance of the order of the contact radius  $a_0$ . This then requires that  $t_0/T \approx a_0/|\xi_0| \ll 1$ . This can be easily shown by estimating the local time derivative and the convective term and requiring that  $\frac{|\partial\sigma/\partial t|}{|\mathbf{v} \cdot \nabla\sigma|} \ll 1$ , i.e.

$$\left| \frac{\partial\sigma}{\partial t} \right| \approx \frac{\sigma_{\max}}{T}; \quad |\mathbf{v} \cdot \nabla\sigma| \approx \frac{\sigma_{\max}}{a_0} \omega |\xi_0|; \quad (12)$$

where  $\sigma_{\max}$  is the maximum contact pressure and, then, by taking the ratio of the derivative terms, one obtains:

$$\frac{|\partial\sigma/\partial t|}{|\mathbf{v} \cdot \nabla\sigma|} \approx \frac{|\partial\sigma/\partial t|}{\omega |\xi_0| \cdot \nabla\sigma} \approx \frac{1}{2\pi} \frac{a_0}{|\xi_0|} \ll 1 \quad (13)$$

At the end of each stroke during reciprocation, the aforementioned condition may look critical since the velocity of the sphere tends to vanish; however, since the time the sphere spends at the dead points of the cyclic sliding motion is also zero, things have to be observed a bit more carefully. Indeed, we can calculate the time  $t_0$  to cover a distance of the order  $a_0$  when the sphere starts moving from the dead point: the distance  $a_0$  can be estimated as  $a_0 \approx (1/2)\omega^2 \xi_0 t_0^2$ . One can, then, easily show that  $t_0/T \approx (a_0/|\xi_0|)^{0.5}$ ; hence, if  $a_0/|\xi_0| \ll 1$ , also  $t_0/T$  will be sufficiently small to justify the constant shape assumption also at the dead points.

Incidentally, we observe that we have numerically checked the condition  $\frac{|\partial\sigma/\partial t|}{|\mathbf{v} \cdot \nabla\sigma|} \ll 1$  for all the cases presented in the main manuscript once the stress distribution was calculated from the solution of Eq. (1).

### Appendix B: Comparison between steady-state and reciprocating contacts

One of the main purposes of this paper is to shed light on the unique features of the viscoelastic reciprocating

contacts. To this aim, it can be useful here to point out the differences between viscoelastic steady-state sliding and reciprocating conditions. From a physical point of view, the two conditions are almost antithetical: in the steady-state case, the punch always meets underformed material [7]; on the contrary, as we explain in the main manuscript, when dealing with reciprocating contacts, the rigid punch may deform a region of material that has not yet relaxed. Only in the limit case of very small values of the parameter  $\Xi$ , i.e. given a relaxation time  $\tau$  for very small frequencies  $\omega$ , the reciprocating case tends to a steady-state-like regime, where the material has got time to relax before the punch re-engages with it.

This physical background entails remarkable differences in terms of interfacial pressures, normal displacements and, consequently, friction. In Fig. 5, we compare the contour plots of the normal pressure for the two cases, i.e. the reciprocating contact conditions and the sliding steady-state contacts. In Fig. (5a), at the inversion point, i.e. when the speed is nominally equal to zero, in the reciprocating case, the pressure still shows a marked asymmetry, that is the consequence of the viscoelastic time-delay which prevents the material to relax immediately when the sliding speed vanishes. On the contrary, in steady-state conditions, the solution at zero speed cannot be anything else than the elastic classic Hertzian solution with the zero-frequency modulus  $E_0$ . Furthermore, given a constant normal load, in this last case, due to the lower modulus, the contact area is much bigger and normal stresses are much smaller. When the punch starts moving back to the right dead point, we still have remarkable differences in the pressure distributions (see Fig. (5b)). Such differences are also clearly perceived when looking at the normal displacements. Upon the motion inversion, we observe the formation of an additional peak in the displacement distribution: this is impossible in steady-state conditions. Different distributions in terms of pressure and normal displacements lead to a different hysteretic curve (see Figure 4 in the main manuscript), thus highlighting the importance of the unique features that characterize reciprocating contact conditions.

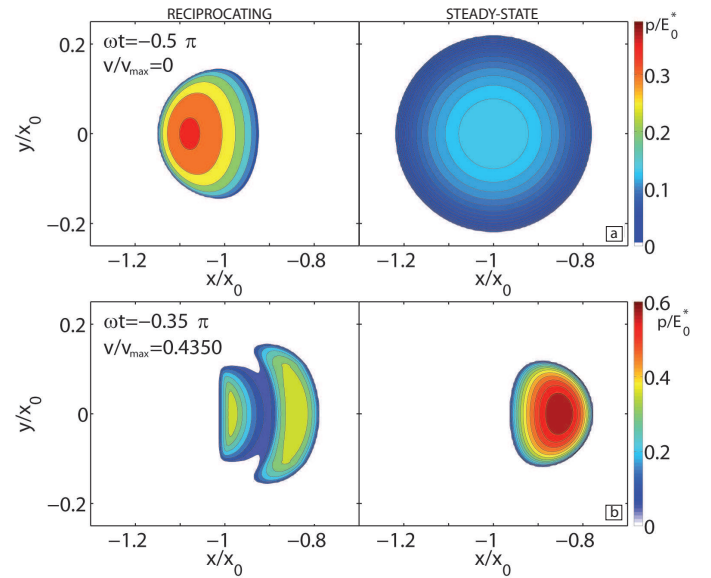


FIG. 5. The shape of the contact area and the contour plots of the normalised contact pressure distributions,  $p/E_0^*$ , in reciprocating (on the left) and steady-state (on the right) conditions for different values of the time and, consequently, of the speed.

---

[1] Arzt E., Gorb S., and Spolenak R., From micro to nano contacts in biological attachment devices. *Proceedings of the National Academy of Sciences*, 16, 100, 19, 10603–10606, (2003).

[2] Bao G., Suresh S., Cell and molecular mechanics of biological materials, *Nature Materials* 2, 715 - 725, (2003).

[3] Johannessen W., Vresilovic E. J., Wright A. C., Elliott D. M., Intervertebral Disc Mechanics Are Restored Following Cyclic Loading and Unloaded Recovery. *Annals of Biomedical Engineering*, 32, 1, 70-76, (2004).

[4] Hunter S.C., The rolling contact of a rigid cylinder with

a viscoelastic half space. *Trans. ASME, Ser. E, J. Appl. Mech.* 28, 611–617 (1961).

[5] Persson B.N.J., Theory of rubber friction and contact mechanics, *Journal of Chemical Physics*, 115, 3840–3861, (2001).

[6] Dapp, W.B., Lücke, A., Persson, B.N.J., Müser, M.H., Self-affine elastic contacts: Percolation and leakage, *Physical Review Letters*, 108 (24), 244301, (2012).

[7] Carbone G., Putignano C., A novel methodology to predict sliding/rolling friction in viscoelastic materials: theory and experiments., *Journal of Mechanics and Physics of Solids*, *Journal of the Mechanics and Physics of Solids*, 61 (8), 1822-1834, (2013).

[8] Grosch K. A., The Relation between the Friction and Visco-Elastic Properties of Rubber, *Proceedings of the Royal Society of London. Series A, Mathematical and Physical*, 274-1356, 21-39, (1963).

[9] Putignano C., Reddyhoff T., Carbone G., Dini D., Experimental investigation of viscoelastic rolling contacts: a comparison with theory. *Tribology Letters*, 51, 105–113, (2013).

[10] Thatte A., Salant R. F., Effects of multi-scale viscoelasticity of polymers on high-pressure, high-frequency sealing dynamics, *Tribology International*, 52, 75–86, (2012).

[11] Shukla A. and Datta T., Optimal Use of Viscoelastic Dampers in Building Frames for Seismic Force. *Journal of Structural Engineering*, 125 (4), 401–409, (1999).

[12] Takewaki I. *Building Control with Passive Dampers: Optimal Performance-based Design for Earthquakes*, John Wiley & Sons, (2011).

[13] Angelini T. E., Dunn A. C., Uruena J. M., Dickrell D. J., Burris D. L. and Sawyer W. G., Cell Friction, *Faraday Discussion*, 156, 31–39, (2012).

[14] Dunn A. C., Cobb J. A., Kantzios A. N., Lee S. J.,

- Sarntinoranont M. , Tran-Son-Tay R. , Sawyer W. G. , Friction Coefficient Measurement of Hydrogel Materials on Living Epithelial Cells, *Tribology Letters*, 30, 1,13-19, (2008).
- [15] Christensen R. M., *Theory of viscoelasticity*, Academic Press, New York, (1982).
- [16] Johnson, K.L.J., *Contact Mechanics*, Cambridge University Press, (1985).
- [17] Putignano C., Afferrante L. , Carbone G., Demelio G. , The influence of the statistical properties of self-affine surfaces in elastic contact: a numerical investigation, *Journal of Mechanics and Physics of Solids*, 60, 5, 973–982, (2012).
- [18] Barber J., *Elasticity*, Kluwer Academic Publisher, (2010).
- [19] Carbone G., Mangialardi L.: Analysis of adhesive contact of confined layers by using a Green’s function approach, *The Journal of the Mechanics and Physics of Solids*, **56** (2), 684-706 (2008)
- [20] C. Putignano, G. Carbone, D. Dini, *Mechanics of Rough Contacts in Elastic and Viscoelastic Thin Layers*, *International Journal of Solids and Structures*, 69–70, 507–517, (2015).